Applied Water Science (2019) 9:41
https://doi.org/10.1007/s13201-019-0919-7

ORIGINAL ARTICLE

Enhanced adsorption of As(III) on chemically modified activated carbon fibers

Jie Shi[1] · Zhiwei Zhao[2] · Jihao Zhou[1,3] · Tianyi Sun[3,4] · Zhijie Liang[2]

Received: 10 February 2016 / Accepted: 4 March 2019 / Published online: 15 March 2019

Abstract

In this study, potentials of Fe- and HNO_3-modified activated carbon fiber (ACF) for the adsorption of As(III) from aqueous solutions were evaluated. The adsorbent was characterized by Brunauer–Emmett–Teller (BET), scanning electron microscopy and X-ray diffraction spectra. It was found that both the modified ACF and unmodified ACF had large specific surface areas. Compared with the unmodified ACF, the crystallinity of the Fe- and HNO_3-modified ACF showed a trend of decrease. The final equilibrium was achieved within approximate 60 min, and the removal of As(III) was significantly influenced by the initial pH. Isotherm simulations revealed that the ACF exhibited effective adsorption capacity for As(III) in aqueous solution. The adsorption isothermal data fitted the Langmuir isotherm model better than the Freundlich isotherm model for the unmodified ACF and HNO_3-modified ACF, but the Freundlich isotherm model was more suitable for the Fe-modified ACF. According to the Langmuir models, the maximum adsorption capacity of As(III) was 2.06, 2.98 and 8.65 mg/g for ACF-0, ACF-1 and ACF-2, respectively. The results demonstrated that the adsorption capacity was enhanced significantly by Fe and HNO_3 modification, and the Fe-modified ACF showed a higher potential for the adsorption of As(III) ion from aqueous solution than the unmodified ACF and HNO_3-modified ACF.

Keywords Activated carbon fiber (ACF) · As(III) · Adsorption · Modification

Introduction

The ubiquitous presence of arsenic ions in natural waters has become an important issue around the world due to its toxic and carcinogenic effect on the aquatic ecological system and human health (Gong et al. 2015; Li et al. 2014). Arsenic contamination problem has been documented in many countries including Argentina, Australia, China, India, Thailand and the USA (Sorlini and Gialdini 2010). Sources of arsenic contamination include both natural and anthropogenic activities, such as fossil fuels, industrial and agricultural waste (Sun et al. 2013; Payne and Abdel-Fattah 2005). Hence, the World Health Organization (WHO) has stipulated that the maximum concentration of arsenic is 10 µg/L in drinking water.

Numerous efforts have been made for developing technologies for arsenic removal, such as chemical coagulation and precipitation, adsorption, membrane separation and ion exchange (Kong et al. 2014; Fu and Wang 2011; Yu et al. 2013). Because of its ease control, simple implement and effective cost, the adsorption is the most widely utilized in the removal of arsenic (Meitei and Prasad 2014; Shih et al. 2015). As a new type of activated carbon, activated

✉ Zhiwei Zhao
hit_zzw@163.com

✉ Zhijie Liang
zhjliang@outlook.com

Jie Shi
shijie8601@sohu.com

Jihao Zhou
jihao2002@163.com

Tianyi Sun
tianyi870328@163.com

1 PLA, No. 93413, Yongji, Shanxi 044500, People's Republic of China

2 College of Urban Construction and Environmental Engineering, Chongqing University, Chongqing 400045, People's Republic of China

3 Department of National Defense Architecture Planning and Environmental Engineering, Logistical Engineering University, Chongqing 401311, China

4 State Key Laboratory of Urban Water Resource and Environment, Harbin Institute of Technology, Harbin 150090, China

carbon fiber (ACF) is considered as a promising adsorption material used for the treatment of wastewater due to the excellent adsorption performances based on its nanostructure, abundant micrometer porosity, high specific surface area and narrow pore size distribution (Rafique et al. 2015). Additionally, the AFC was easily applied in the adsorptive filter for real wastewater treatment. Meanwhile, the adsorption layer would not lead to the increase in resistance or the uneven distribution of the fluid, which were caused by the uneven clastic sediments. Without secondary pollution, ACF is being applied in the water treatment field gradually.

Typically, the surface sites for bonding -OH are the main contribution for the adsorption of arsenic. Hence, various novel materials were synthesized, including rare metal oxides, bimetal oxide composites, ion-exchange resins. However, either the methodological complexity or the high preparation cost limits the wide application of the novel materials in the treatment of the real arsenic contaminated water.

In this study, the modifications with Fe oxide and HNO_3 were applied to ACF to enrich -OH contents for arsenic removal, and the adsorption capacities for As(III) were compared with the unmodified ACF. For the most effective adsorbent, the physical and chemical characteristics were analyzed with BET, SEM and XRD. Furthermore, the effects of the initial pH, the adsorption kinetics and isotherm of As(III) on ACF were evaluated, aiming at providing technical support for the development of the effective adsorbent and giving the scientific theory support for the AFC application in the arsenic contaminated water purification.

Experimental

Materials and reagents

All chemicals used in the experiments were of analytical grade, and all solutions were prepared with Milli-Q water. ACF was purchased from Nantong Sutong Carbon Fiber Co., Ltd., Nantong, China.

ACF was cut into 10 cm × 20 cm pieces, which were then kept in boiling water for 30 min to remove dirt and soluble salts (labeled as ACF-0). The ACF-0 was further cut into 2 cm × 2 cm for use, and the achieved ACF was immersed into 250 mL of the concentrated nitric acid (65–68 wt%) for 120 min at 298 K. The HNO_3-modified ACF (ACF-1) was obtained after washed with distilled water thoroughly and dried in an oven until its mass was constant at 378 K. The achieved ACF was also immersed into 200 mL of aqueous solution containing ferric chloride ($FeCl_3{\cdot}6H_2O$ 160 mL, 0.15 mol/L) and ferrous sulfate ($FeSO_4{\cdot}7H_2O$ 40 mL, 0.15 mol/L) under stirring, and then, 1.0 M sodium hydroxide (NaOH) solution was added dropwise into the mixture with vigorous mechanical stirring till the pH of the supernatant liquid was ranged from 8.0 to 9.0. After pH adjustment, the suspension was continuously stirred for 240 min at 298 K. The Fe-modified ACF (ACF-2) was obtained after washed with distilled water thoroughly and dried in an oven until its mass was constant at 378 K.

Batch sorption experiments

In the As(III) ion adsorption kinetic experiments, a dosage of 500 mg/L ACF was used in 150-ml synthesized As(III)-contained water sample (initial concentrations of 2 mg/L) with shaking at 150 rpm. Samples were taken at regular time intervals.

To examine the effect of pH on As(III) ion adsorption, 50-mL synthesized As(III)-contained water samples (initial concentrations of 2 mg/L) were added in 150-mL Erlenmeyer flasks, and the initial pH was adjusted and measured in the range from 2.00 to 10.00 with 0.1 mol/L HCl or 0.1 mol/L NaOH. After 500 mg/L ACF added, flasks were shaking for 300 min at 303 K and 150 rpm. All experiments were conducted in replicates.

As for isotherm studies, the initial As(III) concentrations were ranged from 5 mg/L to 30 mg/L with adding 500 mg/L ACF. Experiments were conducted with the same method as described above.

Samples were taken with pipettes. After filtered through 0.45-mm microporous membranes, the filtrates were analyzed on an inductively coupled plasma optical emission spectrometer (ICP-OES, PerkinElmer Optima 5300DV, USA) to detect the concentration of As(III).

Characterization

The morphological analysis of the samples was achieved on a FEI Quanta200 microscope, and the crystallographic phase structures of the products were characterized by the X-ray diffraction spectra (XRD) with Cu/Ka radiation ($k = 0.154021$ nm).

Surface areas of the modified and unmodified ACF were measured at 77 K according to Brunauer–Emmett–Teller (BET) multipoint technique through an ASAP 2020, and the features of pore structure were determined based on Barrett, Joyner and Halenda (BJH) method and t-plot.

Data analysis

The sorption capacity q (mg/g) was calculated by the following equation (Futalan et al. 2011):

$$q = \left[\left(C_0 - C_d\right)V/W\right] \quad (1)$$

where C_0 and C_d are the initial and detected concentrations (mg/L) of As(III) in the aqueous solution, respectively. V is

the volume of the synthesized As(III)-contained water, and W is the weight of ACF.

The Langmuir model (Eq. 2) and the Freundlich model (Eq. 3) were used for the analysis of the adsorption isotherm data.

$$Q_e = b \cdot q_{max} v C_e / \left(1 + b \cdot C_e\right) \quad (2)$$

$$Q_e = K_f \cdot C_e^{1/n} \quad (3)$$

where Q_e is the tested equilibrium adsorption capacity and q_{max} is the theoretical maximum adsorption capacity. In Eq. (2), parameter b is the Langmuir constant reflecting the binding site affinity. In Eq. (3), K_f is the Freundlich constant related to adsorption capacity, and parameter n reflects the adsorption intensity.

Results and discussion`

Material characterizations

BET analysis

The surface areas and pore diameters determine the adsorption properties of adsorbent. ACF had a plenty of inner pore, giving a large specific surface area. As presented in Table 1, the BET surface areas for all ACF samples were above 1200 m^2/g. The BET surface area, the BJH average pore diameter and the pore volume of the modified ACF by HNO_3 and Fe changed in different degrees. Under normal temperature conditions, the concentrated HNO_3 dissolved some ash content on the surface of ACF, which was helpful for the further expansion of porous structure. However, the concentrated HNO_3 also corroded the structure of ACF, which partly collapsed the internal channel structure and decreased the specific surface of ACF. As for the Fe-modified ACF, a layer of Fe material loaded on inner surface clogged some channels and reduced the specific surface area, the average pore diameter and the pore volume accordingly (Rey et al. 2009; Sigrist et al. 2014).

Figure 1 shows the pore size distributions of ACF. As shown in Fig. 1, the pore diameters of ACF were between 1 and 20 nm. Meanwhile, all the nitrogen adsorption/desorption curves of the three types of ACF were correspondence to the Type IV adsorption isotherm. Since the mesopore was defined as 2–50 nm by IUPAC, the unmodified and Fe-modified AFC was microporous, but HNO_3 modification enlarged the pore structure and resulted in a mesoporous structure, based on the calculation result in Table 1. Hence, ACF showed the micropore/mesopore structure characteristics and might serve as a promising material for the adsorption of As(III) in water.

Table 1 Selected properties of ACF-0, ACF-1 and ACF-2 series of samples

Sample	S_{BET} (m^2/g)	D_P (nm)	V_{total} (cm^3/g)
ACF-0	1281.57	1.93	0.62
ACF-1	1216.85	2.13	0.65
ACF-2	1237.60	1.84	0.57

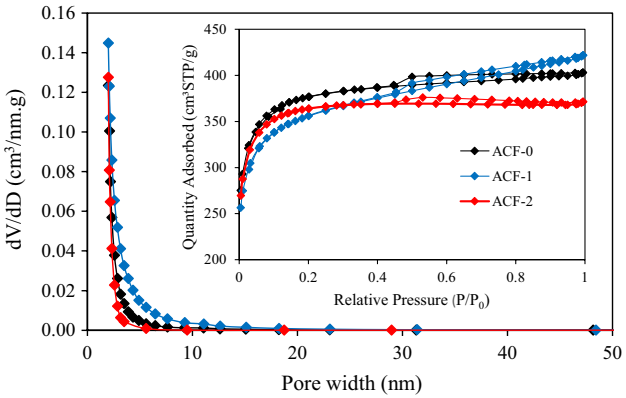

Fig. 1 Pore size distributions of ACF-0, ACF-1 and ACF-2. The inset shows the variation in the mesoporous and microporous character of nitrogen adsorption/desorption isotherms

Morphology of the adsorbent

Figure 2a shows the SEM image of original ACF, and it indicated that the surface of ACF was fluted and smooth on the whole, in which there were a few cracks and small spots (Fig. 2b). The surface morphologies of HNO_3 and Fe-modified ACF were changed to be rough, especially for ACF-2 (Fig. 2c), and the surface was covered by floccule with diameters at about hundreds of nanometer. As shown in Fig. 2d, the EDX analysis demonstrated that the main elements were C, O, and Fe. It was in accordance with the phenomenon observed by Xu et al. (2013) that there was a layer of iron nanoparticles about 20–80 nm loaded on the surface of the activated carbon.

XRD analysis

The XRD patterns of the ACF-0, ACF-1 and ACF-2 are shown in Fig. 3. As shown in Fig. 3, three types of ACF showed the diffraction peak C (002) with graphitized characteristics. For the HNO_3 and Fe-modified ACF, the diffraction peak C (002) becomes wide and short, which indicated that the crystallization degrees of ACF-1 and ACF-2 showed a trend of decrease and presented the trend of moving to the right. Meanwhile, the small graphite plane peak C (101) was detected at 44.8° (θ), and the strength of the diffraction

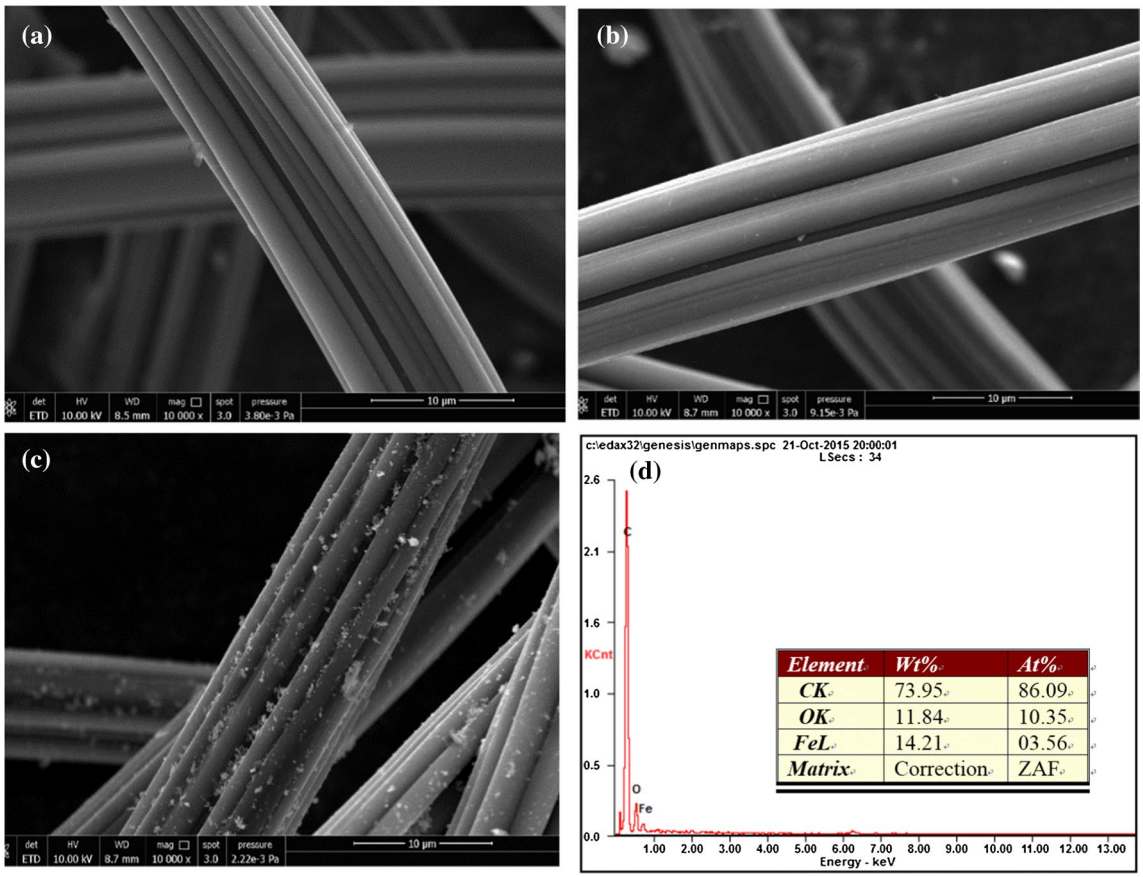

Fig. 2 SEM images of **a** ACF-0, **b** ACF-1, **c** ACF-2, **d** EDAX spectra of ACF-2

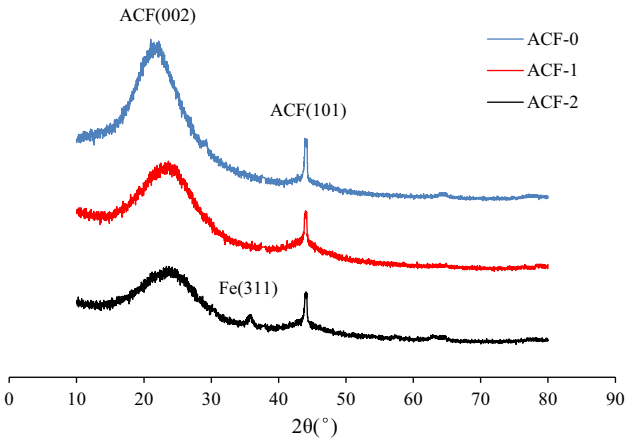

Fig. 3 XRD analysis of ACF-0, ACF-1 and ACF-2

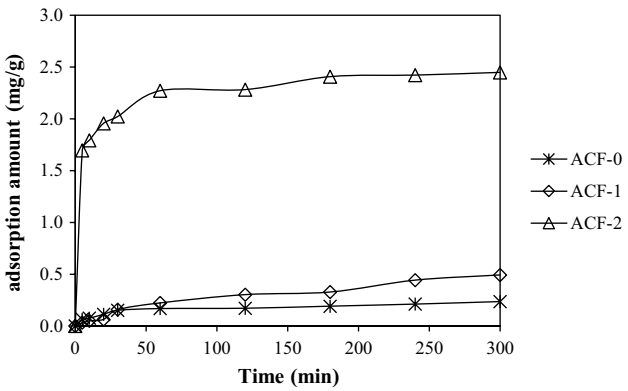

Fig. 4 Adsorption kinetics of As(III) by ACF. Concentration of As(III) was 2 mg/L; dosages of absorbents were 500 mg/L, and the initial pH was 6.0

peaks C (101) showed a decrease for the HNO_3 and Fe-modified ACF. Hence, ACF is an amorphous material made up of some graphite minicrystals (Peng et al. 2015), and the modification was the process of pore etching actually. In addition, a diffraction peak Fe (311) appears in ACF-2, which is Fe_3O_4 characteristic peak (Li et al. 2015).

Adsorption kinetics

Adsorption kinetics are mainly used to determine the retention time of adsorption process. Figure 4 shows the adsorption kinetics of As (III) on ACF. As represented in Fig. 4, the adsorption of As (III) increased with the increase in

contact time, and the adsorption equilibrium time was fixed at 60 min considering the treatment efficiency. Compared with the adsorption process of ACF-0, the adsorption equilibrium time increased after Fe and HNO_3 modification, but the adsorption capacities were 0.236 mg/g, 0.493 mg/g and 2.45 mg/g at 300 min, respectively. Therefore, the Fe-modified ACF effectively improved the adsorption capacities on As (III) removal.

The experimental results were consistent with Mondal et al (2013) who reported that Fe^{3+} impregnated granular activated charcoal (GAC-Fe) was more efficient for the treatment of As ions contaminated groundwater.

Effect of pH

The pH of the solution plays an important role in the surface complexation between adsorbents and arsenic(III) (Cao et al. 2014). Effect of pH on the adsorptive removal of As(III) onto ACF is presented in Fig. 5. Figure 5a shows that the removal efficiencies by ACF-0, ACF-1 and ACF-2 increased sharply from 1.26 to 66.04%, 0.51 to 57.83% and 6.66 to 74.44% with the pH increased from 2.83 to 9.54. However, when the pH was higher than 5.5, the adsorption capacity of ACF-1 was less than that of ACF-0 and ACF-2.

To examine the mechanism of pH effect, the pH_{PZC} (the potential of zero charged) of the unmodified and modified AFC was measured. As shown in Fig. 5b, the pH_{PZC} of ACF-0 and ACF-2 was maintained between 3.66 and 5.5, while the pH_{PZC} of ACF-1 was maintained between 2.83 and 3.66. Due to the fact that ACF-1 has the smallest pH_{PZC} value, the negative charge on the surface increased with the pH increase, and the continuous increase in negative charge produced electrostatic repulsion with As (III) negative ion. Hence, the adsorption capacity of ACF-1 was less than ACF-0 and ACF-2 when the pH was higher than 5.5. These results are in good agreement with literature since they show that As (III) adsorption was pH dependent (Veličković et al. 2012; Mamindy-Pajany et al. 2011).

Hence, based on the pH_{pzc} studies and pH effect evaluation, a higher pH_{pzc} was optimal, and the quantified target pH value range was from 5.0 to 6.0 for the removal of As from waters.

Adsorption isotherm

Adsorption isotherm is a powerful tool to study the adsorption capacities of adsorbents. The adsorption parameters were determined by the linearized Langmuir and Freundlich

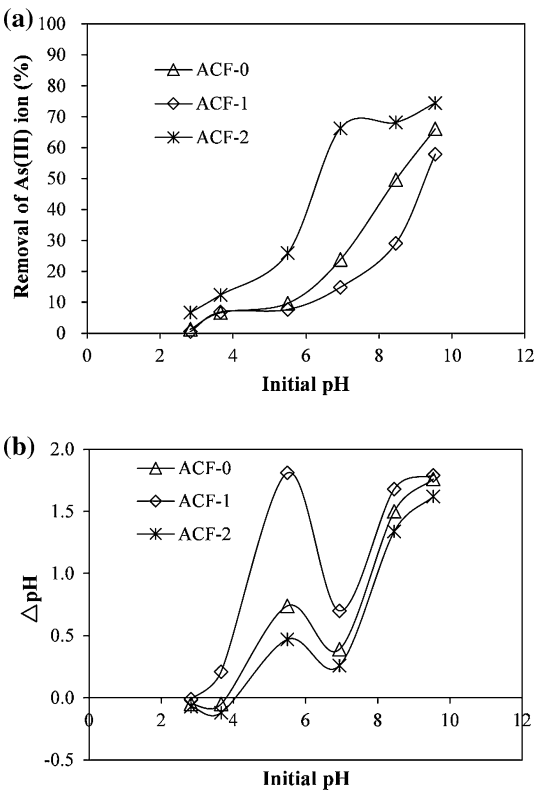

Fig. 5 Effect of the initial pH on the adsorption of As (III) by ACF-0, ACF-1 and ACF-2. Dosages of absorbents were 500 mg/L; concentration of As (III) was 2 mg/L; and reaction time was 300 min

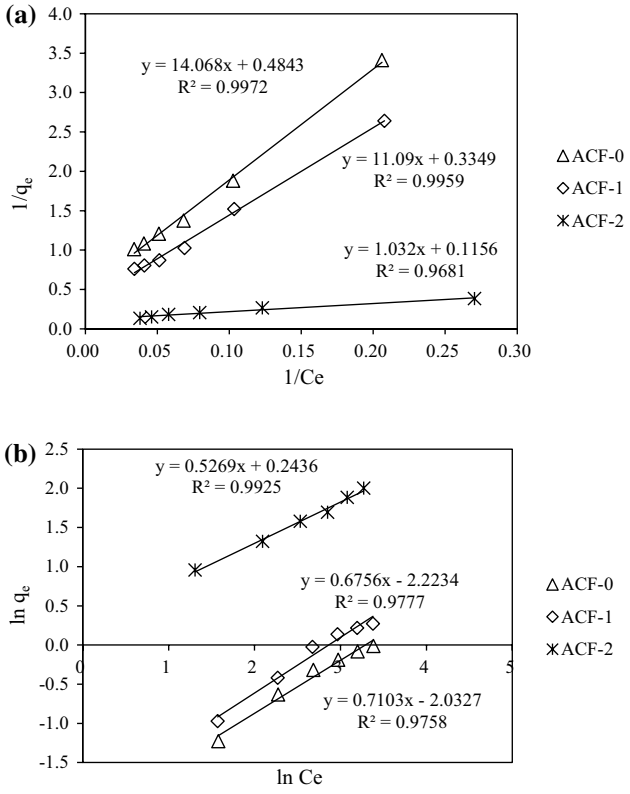

Fig. 6 Linearized adsorption isotherms of As (III) by ACF-0, ACF-1 and ACF-2: Langmuir (**a**) and Freundlich (**b**). Dosages of absorbents were 500 mg/L; reaction time was 300 min, and the initial pH was 6.0

Table 2 Values of adsorption parameters obtained from the Langmuir and Freundlich models with the different ACFs (ACF-0, ACF-1 and ACF-2)

Adsorbent	Langmuir			Freundlich		
	q_m (mg/g)	K_L (L/mg)	R^2	K_F (mg/g)	1/n	R^2
ACF-0	2.06	0.034	0.9927	0.13	0.7103	0.9758
ACF-1	2.98	0.030	0.9959	0.11	0.6756	0.9777
ACF-2	8.65	0.112	0.9681	1.28	0.5269	0.9925

isothermal adsorption models, which were based on the theory of monolayer adsorption and multiphase adsorption, respectively. Each isotherm model was expressed by relative certain constants, which characterized the surface properties and the adsorption capacity of the adsorbent (Aljeboree et al. 2014; Shi et al. 2015).

Figure 6 illustrates the Langmuir and Freundlich adsorption isotherms of As(III) onto ACF. The adsorptions of As(III) on the ACF-0 and ACF-1 were correlated better with the Langmuir isotherm model than those with the Freundlich isotherm model, which suggested that the adsorption of As(III) belonged to the homogeneous adsorption process (Li et al. 2003). As for the ACF-2 adsorbent, the redox reactions took place in the As(III) adsorption process, which was a heterogeneous adsorption process contributed by the loading of Fe oxide. Hence, the obtained equilibrium data of As(III) fitted perfectly with Freundlich isotherm model compared with Langmuir isotherm model.

The Langmuir and Freundlich isotherm parameters were calculated and are listed in Table 2. The adsorptive capacities for As (III) ion removal were in the order of ACF-2>ACF-1>ACF-0, which was because of that a large number of As(III) was translated into As(V) during adsorption process with the Fe-modified ACF. Most of the As(III) was in the presence of molecular form in the source water, while As(V) was in the ion form, so the adsorbent has much higher affinity to As(V) than to As(III) (Zhao et al. 2012; Morillo et al. 2015). Based on the Langmuir isotherm model, the maximum adsorption capacities of As(III) on ACF-0, ACF-1 and ACF-2 were 2.06, 2.98 and 8.65 mg/g, respectively, which suggested that the modified ACF adsorbent by Fe removed As(III) efficiently from the aqueous solution.

Conclusion

The adsorption of As(III) onto three types of ACF was investigated in the single metal solution system. ACF had a large specific surface area and pore volume, but HNO_3 modification corroded the inner channel of the ACF, and the Fe modification plugged the channel, both of which made the specific surface area reduced. The HNO_3 and Fe modifications have increased surface roughness of ACF. The adsorption equilibrium time was 60 min, and the adsorption equilibrium time increased after Fe and HNO_3 modifications. The adsorption isothermal data fitted with the Langmuir isotherm model better than the Freundlich isotherm model. Conclusively, these preliminary results indicated that the ACF showed a promising prospect for the treatment of the As(III)-contaminated water and wastewater, and the adsorption capacity was enhanced significantly by Fe and HNO_3 modifications.

Acknowledgements This research study was supported by the National Natural Science Foundation of China (No. 51808066), the Fundamental Research Funds for the Central Universities (No. cqu2018CDHB1A10) and the Project No. 2018CDXYCH0013 Supported by the Fundamental Research Funds for the Central Universities.

References

Aljeboree AM, Alshirifi AN, Alkaim AF (2014) Kinetics and equilibrium study for the adsorption of textile dyes on coconut shell activated carbon. Arab J Chem 5:2. https://doi.org/10.1016/j.arabjc.2014.01.020

Cao F, Yin P, Zhang J, Chen H, Qu R (2014) Nanoplates of cobalt phosphonate with two-dimensional structure and its competitive adsorption of Pb(II) and Hg(II) ions from aqueous solutions. J Ind Eng Chem 20:2568–2573

Fu F, Wang Q (2011) Removal of heavy metal ions from wastewaters: a review. J Environ Manag 92(3):407–418

Futalan CM, Kan CC, Dalida ML, Hsien KJ, Pascua C, Wan MW (2011) Comparative and competitive adsorption of copper, lead, and nickel using chitosan immobilized on bentonite. Carbohydr Polym 83(2):528–536

Gong XJ, Li WG, Zhang DY, Fan WB, Zhang XR (2015) Adsorption of arsenic from micro-polluted water by an innovative coal-based mesoporous activated carbon in the presence of co-existing ions. Int. Biodeterior Biodegrad. https://doi.org/10.1016/j.ibiod.2015.01.007

Kong Z, Li X, Tian J, Yang J, Sun S (2014) Comparative study on the adsorption capacity of raw and modified litchi pericarp for removing Cu (II) from solutions. J Environ Manag 134:109–116

Li YH, Ding J, Luan Z, Di Z, Zhu Y, Xu C, Wu D, Wei B (2003) Competitive adsorption of Pb^{2+}, Cu^{2+} and Cd^{2+} ions from aqueous solutions by multiwalled carbon nanotubes. Carbon 41:2787–2792

Li WG, Gong XJ, Wang K, Zhang XR, Fan WB (2014) Adsorption characteristics of arsenic from micro-polluted water by an

innovative coal-based mesoporous activated carbon. Bioresou Technol 165:166–173

Li S, Zhang T, Tang R, Qiu H, Wang C, Zhou Z (2015) Solvothermal synthesis and characterization of monodisperse superparamagnetic iron oxide nanoparticles. J Magn Magn Mater 379:226–231

Mamindy-Pajany Y, Hurel C, Marmier N, Roméo M (2011) Arsenic (V) adsorption from aqueous solution onto goethite, hematite, magnetite and zero-valent iron: effects of pH, concentration and reversibility. Desalination 281:93–99

Meitei MD, Prasad MNV (2014) Adsorption of Cu (II), Mn(II) and Zn (II) by Spirodela polyrhiza (L.) Schleiden: equilibrium, kinetic and thermodynamic studies. Ecol Eng 71:308–317

Mondal P, Mohanty B, Majumder CB (2013) Effect of pH and treatment time on the removal of arsenic species from simulated groundwater by using Fe^{3+} and Ca^{2+} impregnated granular activated charcoals. Chem Eng Sci 1(2):27–31

Morillo D, Pérez G, Valiente M (2015) Efficient arsenic (V) and arsenic (III) removal from acidic solutions with Novel Forager Sponge-loaded superparamagnetic iron oxide nanoparticles. J Colloid Interface Sci 453:132–141

Payne KB, Abdel-Fattah TM (2005) Adsorption of arsenate and arsenite by iron-treated activated carbon and zeolites: effects of pH, temperature, and ionic strength. J Environ Sci Health 40(4):723–749

Peng L, Chen Y, Dong H, Zeng Q, Song H, Chai L, Gu JD (2015) Removal of trace As (V) from water with the titanium dioxide/ACF composite electrode. Water Air Soil Pollut 226(7):1–11

Rafique RF, Min Z, Son G, Lee SH (2015) Removal of cadmium ion using micellar-enhanced ultrafiltration (MEUF) and activated carbon fiber (ACF) hybrid processes: adsorption isotherm study for micelle onto ACF. Desalin Water Treat. https://doi.org/10.1080/19443994.2015.1057538

Rey A, Faraldos M, Casas JA, Zazo JA, Bahamonde A, Rodríguez JJ (2009) Catalytic wet peroxide oxidation of phenol over Fe/AC catalysts: influence of iron precursor and activated carbon surface. Appl Catal B-Environ 86(1–2):69–77

Shi J, Fang Z, Zhao Z, Sun T, Liang Z (2015) Comparative study on Pb(II), Cu (II), and Co (II) ions adsorption from aqueous solutions by arborvitae leaves. Desalin Water Treat. https://doi.org/10.1080/19443994.2015.1089421

Shih YJ, Huang RL, Huang YH (2015) Adsorptive removal of arsenic using a novel akhtenskite coated waste goethite. J Clean Prod 87:897–905

Sigrist ME, Brusa L, Beldomenico HR, Dosso L, Tsendra OM, González MB, Pieck CL, Vera CR (2014) Influence of the iron content on the arsenic adsorption capacity of Fe/GAC adsorbents. J Environ Chem Eng 2(2):927–934

Sorlini S, Gialdini F (2010) Conventional oxidation treatments for the removal of arsenic with chlorine dioxide, hypochlorite, potassium permanganate and monochloramine. Water Res 44(19):5653–5659

Sun Z, Yu Y, Pang S, Du D (2013) Manganese-modified activated carbon fiber (Mn-ACF): novel efficient adsorbent for Arsenic. Appl Surf Sci 284:100–106

Veličković Z, Vuković GD, Marinković AD, Moldovan MS, Perić-Grujić AA, Uskoković PS, Ristić MĐ (2012) Adsorption of arsenate on iron (III) oxide coated ethylenediamine functionalized multiwall carbon nanotubes. Chem Eng J 181:174–181

Xu JH, Gao NY, Deng Y, Xia SQ (2013) Nanoscale iron hydroxide-doped granular activated carbon (Fe-GAC) as a sorbent for perchlorate in water. Chem Eng J 222:520–526

Yu Y, Zhao C, Wang Y, Fan W, Luan Z (2013) Effects of ion concentration and natural organic matter on arsenic (V) removal by nanofiltration under different transmembrane pressures. J. Environ. Sci 25(2):302–307

Zhao Z, Liu J, Cui F, Feng H, Zhang L (2012) One pot synthesis of tunable Fe_3O_4-MnO_2 core-shell nanoplates and their applications for water purification. J Mater Chem 22(18):9052–9057